

## Synthesis and Characterization of Cellulose Nanocrystals from Alkali-Pretreated *Parthenium hysterophorus* with Adsorption Kinetic Studies

DIVYA GAUTAM<sup>1,\*</sup>, YOGESH KUMAR WALIA<sup>1</sup> and VISHAL RANA<sup>2</sup>

<sup>1</sup>Department of Chemistry, School of Basic & Applied Sciences, Career Point University, Hamirpur-176041, India

<sup>2</sup>Department of Chemistry, Thakur P.G. College of Education, Dhaliara, Kangra-177103, India

\*Corresponding author: E-mail: [gautamdivya167@gmail.com](mailto:gautamdivya167@gmail.com)

Received: 8 November 2024;

Accepted: 23 December 2024;

Published online: 31 January 2025;

AJC-21884

This study investigates the synthesis and comprehensive characterization of cellulose nanocrystals (CNC) derived from *Parthenium hysterophorus* biomass through acid hydrolysis. Acid hydrolysis of cellulose extracted from *Parthenium* resulted in a significant increase in crystallinity, as confirmed by X-ray diffraction (XRD), with the nanocellulose exhibiting a crystallinity index of 77%. SEM images revealed that acid hydrolysis resulted in the alteration of the fibrous and coiled structure of cellulose, resulting in the formation of spherical cellulose nanocrystals. The TEM analysis of cellulose nanocrystals revealed an average diameter of approximately 36-79 nm, demonstrating the impact of acid hydrolysis on morphology. Further the structural characterization using FTIR indicated the preservation of cellulose chemical structure, while thermogravimetric analysis (TGA) showed improved thermal stability of the nanocellulose compared to raw biomass post-processing. Zeta potential analysis highlighted strong colloidal stability with a highly negative surface charge ( $-28.9 \pm 6.18$  mV), essential for applications requiring dispersion stability. In adsorption studies, the synthesized nanocellulose effectively removed 75% of malachite green dye from aqueous solutions at room temperature, following pseudo second-order kinetics. This study underscores the potential of *Parthenium*-derived nanocellulose in sustainable materials applications, leveraging invasive weed biomass for eco-friendly nanomaterial production. The findings contribute to advancing sustainable materials research by demonstrating the utility of *Parthenium* biomass for value-added nanomaterial production, specifically highlighting the enhanced properties and effective adsorption capabilities of the synthesized nanocellulose.

**Keywords:** Biomass, Cellulose nanocrystals, Adsorption capabilities, Morphology, Sustainable.

### INTRODUCTION

Nanocellulose, derived from cellulose fibers, has emerged as a pivotal nanomaterial due to its sustainable nature and versatile properties, fostering innovation across diverse industries such as biomedicine, packaging and renewable energy [1]. Nanocellulose, which is well-known for its mechanical strength, biocompatibility and huge surface area, presents a promising platform for developing cutting-edge materials with specialized applications [2].

The synthesis of cellulose nanocrystals (CNCs) is a focal point of current research, aiming to develop efficient methods for producing nanocellulose with desired characteristics. Various methods including mechanical processing, chemical hydrolysis and biological methods have been explored to influ-

ence cellulose nanocrystals properties such as size, shape and crystallinity [3]. Acid hydrolysis, in particular, utilizing strong acids like sulfuric acid, stands out as a prevalent method for generating cellulose nanocrystals from cellulose sources due to its high yield and tunable properties [4].

Cellulose nanocrystals can be sourced from diverse materials including wood, non-wood fibers and agricultural residues such as rice straw and sugarcane bagasse [5,6]. *Parthenium hysterophorus*, an invasive weed abundant in many regions, represents an intriguing biomass source for nanocellulose production. Despite its ecological impact, *Parthenium* biomass offers substantial cellulose content, making it an attractive feedstock for sustainable materials [7]. In this study, cellulose nanocrystals were synthesized *via* acid hydrolysis using cellulose extracted from *Parthenium hysterophorus* biomass. This

study explores the potential of *Parthenium* derived nanocellulose as a sustainable biomaterial, leveraging the abundance of *Parthenium* biomass and the efficiency of acid hydrolysis. The structural properties, morphology, crystallinity and thermal stability of the resulting cellulose nanocrystals were comprehensively characterized, contributing to advancements in sustainable materials research and biomass utilization strategies. Moreover, this study investigates the application of *Parthenium* derived cellulose nanocrystals in wastewater treatment, specifically focusing on their effectiveness as adsorbents for malachite green dye removal. Cellulose nanocrystals have shown promise in water purification applications due to their high surface area and surface chemistry, which facilitate efficient adsorption of pollutants [8]. By elucidating the adsorption kinetics and mechanisms, this study aims to demonstrate the feasibility of utilizing *Parthenium* derived cellulose nanocrystals as eco-friendly method for wastewater treatment, thereby addressing environmental challenges associated with dye pollution.

## EXPERIMENTAL

Plant material of *Parthenium hysterophorus* L. as cellulose source was collected from Kangra valley (middle Himalayas), India (32°05'05"N 76°15'14"E). All the chemicals and reagents employed in this study were of analytical grade and used in their original reagent grade form without further purification. These included NaOH, NaClO<sub>2</sub>, H<sub>2</sub>SO<sub>4</sub>, isopropyl alcohol, ethylene glycol, ethanol, 100% acetic acid, malachite green dye (HiMedia, India). Additionally, double distilled water was utilized exclusively in all the experimental procedures.

**Pretreatment of plant biomass:** The plant biomass pretreatment involved alkali treatment, delignification and bleaching. *P. hysterophorus* plant material was washed, dried and finely ground into powder. It underwent a 24 h alkali treatment using 4% NaOH to remove impurities, followed by thorough washing until neutral. Then, it was bleached with a 1.7% sodium chlorite solution in a pH 4 acetic acid buffer for 4 h [9]. After filtration, neutral pH washing and air-drying, a white cellulose was obtained.

Cellulose content was also determined using equation [10]:

$$\text{Cellulose (\%)} = \frac{m}{M} \times 100 \quad (1)$$

where 'm' represented the mass of white powder obtained and 'M' stood for the original mass of sample.

**Synthesis of cellulose nanocrystals:** Cellulose nanocrystals (CNC) were produced *via* sulfuric acid hydrolysis [4]. The cellulose powder was added gradually to 50 mL of 60 wt.% H<sub>2</sub>SO<sub>4</sub> and stirred for 1 h at room temperature. Hydrolysis was halted by adding 500 mL of iced water. After centrifugation, the sediment containing cellulose nanocrystals was washed until the pH became neutral, then sonicated for 0.5 h. The resulting suspension was centrifuged and the supernatant containing cellulose nanocrystals was collected. This process of sonication and centrifugation was repeated followed by freeze-drying to get cellulose nanocrystals.

**Characterization:** The synthesized cellulose nanocrystals underwent examination through FTIR spectroscopy, SEM and

XRD techniques to discern the structural characteristics of the precursor involved in subsequent reactions. FTIR spectra were acquired using a Perkin-Elmer FTIR spectrophotometer, covering the 4000–400 cm<sup>-1</sup> range and employing the KBr pellet method. The XRD patterns were obtained with a Philips PAN-Analytica XPERT-PRO X-ray diffractometer using CuK $\alpha$  radiation ( $\lambda$  1.54060 Å), with the diffraction angle 2 $\theta$  ranging from 10° to 70°. The morphologies of the resulting cellulose nanocrystals were evaluated by analyzing SEM images captured with an SEM Quanta 250 D9393 and TEM analysis was also performed for morphology measurement using Philips CM 200. Thermogravimetric analysis was conducted using a Perkin Elmer STA 6000 at a heating rate of 10 °C min<sup>-1</sup> under a N<sub>2</sub> atmosphere. Particle size distribution was determined using a Malvern nanosizer (Nano S90 version 7.02). Zeta potential measurements were carried out utilizing a Zeta – 90Plus particle size analyzer from Brookhaven Instruments Corporation, employing suspensions of various prepared samples in water.

**Adsorption studies:** Cellulose nanocrystals was evaluated as an adsorbent for malachite green (MG) dye. Dye concentrations were measured using a PhotoLab 6600 UV-vis spectrophotometer instrument at  $\lambda_{\text{max}} = 617$  nm, the maximum wavelength absorbance for malachite green dye. The malachite green stock solution was prepared at a concentration of 1000 mg/L using distilled water. Working solutions ranging from 10 mg/L to 150 mg/L were then prepared by diluting this stock solution prior to conducting batch adsorption experiments. The impact of contact time was investigated through adsorption studies conducted on cellulose nanocrystals with malachite green dye across various initial dye concentrations. Initially, 10 mg sample was immersed in dye solutions with concentrations of 30 ppm, 50 ppm, 70 ppm, 100 ppm and 120 ppm at 25 °C, neutral pH for durations ranging from 10 to 120 min. After adsorption, C<sub>e</sub> (mg/L) represented the dyestuff concentration, used to calculate q<sub>e</sub> (mg/g), the equilibrium adsorption concentration of the dyestuff. The equations used to evaluate the adsorption capacity at any specific time (q<sub>t</sub>) and the removal efficiency (%) are as follow [8]:

$$q_t = \frac{(C_o - C_e)V}{w} \quad (2)$$

$$R (\%) = \frac{C_o - C_e}{C_o} \times 100 \quad (3)$$

where q<sub>t</sub> represents the quantity of dye adsorbed per unit mass of the adsorbent when dry (mg/g); C<sub>o</sub> stands for the initial dye concentration (mg/L); C<sub>e</sub> denotes the equilibrium dye concentration at time t (mg/L); V indicates the volume of dye solution used (L); and w signifies the mass of the adsorbent (g).

## RESULTS AND DISCUSSION

The preparation process to isolate cellulose and synthesize cellulose nanocrystals (CNC) from *Parthenium hysterophorus* involved several sequential steps. Initially, cellulose was extracted from the natural biomass by eliminating lignin, hemicellulose and other impurities. The enhanced cellulose content

in biomass (43.28%) revealed *P. hysterophorus* as a feasible and plentiful source for nanocellulose synthesis. Subsequent alkali treatment effectively removed extractives such as lignin, hemicellulose, pectin and wax, crucially without significantly affecting the cellulose content. This chemical pretreatment was fundamental in eliminating non-cellulosic constituents from the *P. hysterophorus* fiber, thereby facilitating the isolation of cellulose nanocrystals (CNC) using acid hydrolysis, essential for advanced applications in various fields.

**FTIR spectral studies:** In FTIR spectra (Fig. 1), the peaks observed around  $3416\text{ cm}^{-1}$  and  $2903\text{ cm}^{-1}$  were attributed to the stretching vibrations of O-H bonds and C-H bonds, respectively, characteristic of aliphatic moieties present in polysaccharides [11]. The band observed at  $1734\text{ cm}^{-1}$  was assigned to the ester linkage of carboxylic groups of ferulic and *p*-coumaric acids found in lignin, while the peak at  $1510\text{ cm}^{-1}$  was associated with the stretching vibrations of C=C bonds within the aromatic rings of lignin. In contrast to the spectrum of plant biomass, cellulose exhibited an absence of peaks at  $1734\text{ cm}^{-1}$ , indicating the removal of amorphous components (such as hemicellulose, lignin, pectin and wax) during the alkali pretreatment and bleaching processes [4]. The appearance of a peak at  $1216\text{ cm}^{-1}$  of cellulose nanocrystals was due to the addition of sulfate groups during the sulfuric acid hydrolysis process [12].

**XRD studies:** XRD patterns were used to investigate the crystallite size (*D*) by using the Debye-Scherrer equation [13]:

$$D = \frac{0.94\lambda}{\beta \cos\theta} \quad (4)$$

where  $\lambda = 1.5406\text{ \AA}$  is the wavelength used during XRD analysis;  $\beta$  is the full width at half maximum (FWHM) for the most intense peak;  $\theta$  is Bragg's angle.

The crystallinity index (CI) was derived using the formula derived by equation [14]:

$$CI = \frac{I_{002} - I_{am}}{I_{002}} \times 100 \quad (5)$$

where  $I_{002}$  is the maximum intensity of diffraction of the (002) lattice peak at a  $2\theta$  angle typically between  $22^\circ$  and  $23^\circ$ ;  $I_{am}$  is the intensity of diffraction of the amorphous material, usually measured at a  $2\theta$  angle between  $18^\circ$  and  $19^\circ$  where the intensity is at its minimum.

The results derived from XRD pattern suggested that the acid treatment digested the amorphous regions effectively (Fig. 2). For comparison purposes, XRD results of both plant biomass and cellulose were examined. The XRD pattern of plant biomass exhibited a broad and diffused spectrum, indicating predominantly amorphous material. The observed peaks at  $2\theta = 15.9^\circ$ ,  $22.4^\circ$  and  $34.4^\circ$  were assigned to the (110), (200) and (004) planes, respectively [15,16]. The intensity of these peaks increased and the peaks became sharper in the XRD pattern of the obtained cellulose nanocrystals, signifying a significant enhancement compared to cellulose [17,18].

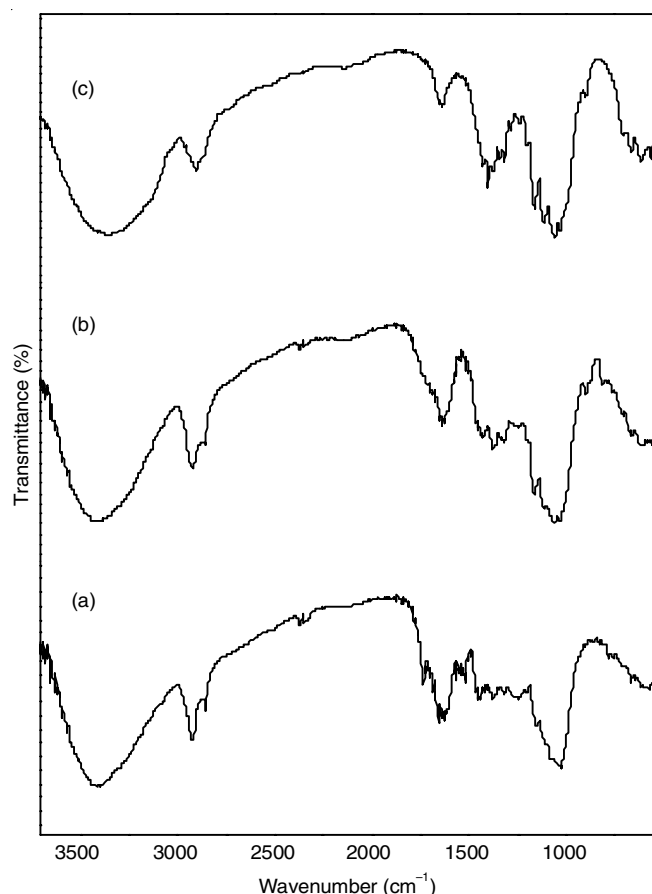


Fig. 1. FTIR spectra of (a) plant biomass, (b) cellulose and (c) cellulose nanocrystals

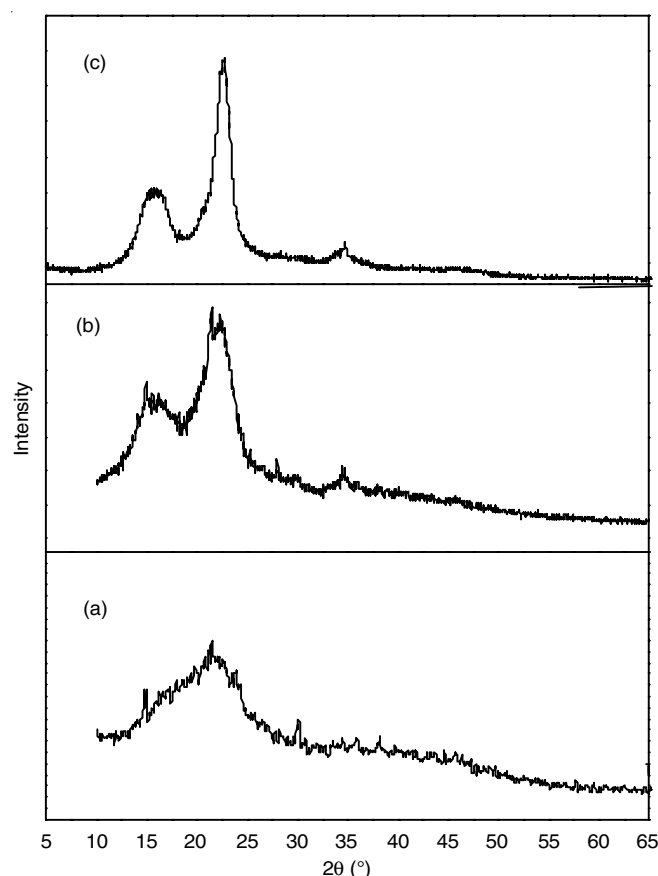


Fig. 2. XRD patterns of (a) plant biomass, (b) cellulose and (c) cellulose nanocrystals

The crystallite size was determined from the prominent (200) peak, calculating a size of 4.979 nm. The *d*-spacing of the crystals at this peak was measured as 3.93 Å. The synthesized cellulose nanocrystals exhibited a crystallinity of 77.32% in comparison to cellulose and plant biomass having CI 53.46 and 23.38%, respectively [19]. The results indicated marked rise in CI of cellulose nanocrystals as compared to plant biomass and cellulose, suggesting that the acid treatment effectively removed amorphous hemicelluloses and defective regions from the cellulose [20,21]. The structural parameters and the crystallinity index (CI) values obtained from XRD are presented in Table-1. Also the obtained results are compared with literature presented in Table-2.

**Morphological studies:** The initial plant biomass exhibited a compact, rough surface morphology. However, following the

Sample	D (nm)	d (nm)	CI (%)
Plant Biomass	31.145	4.872	23.38
Cellulose	25.199	4.349	53.46
Cellulose nanocrystals	4.979	3.915	77.32

Material	d (nm)	CI (%)	Ref.
Cellulose nanocrystals from Garlic straw	480	68.80	[16]
Cellulose nanocrystals from Groundnut shell	111	74.00	[17]
Cellulose nanocrystals from <i>Calotropis procera</i>	250	68.70	[4]
Cellulose nanocrystals from waste cellulose	50	81.23	[15]
Modified cellulose nanocrystals	7.06	74.90	[18]
Cellulose nanocrystals from Rice Straw	28-82	58.43	[19]
Cellulose nanocrystals from tea stalk	4-8	–	[20]
Cellulose nanocrystals ( <i>Eragrostis teff</i> straw)	101	77.10	[21]
Cellulose nanocrystals from <i>Parthenium</i>	4.97	77.32	This study

delignification and bleaching processes, the structure loosened, revealing a fibrous morphology where cellulose fibers were coiled within long tubes (Fig. 3). This change can be attributed to the removal of lignin and hemicellulose from the plant biomass.

The SEM images of cellulose nanocrystals revealed a notable alteration in the shape of the nanoparticles due to acid hydrolysis of cellulose (Fig. 4).

With an acid concentration of 60%, complete removal of the amorphous phase from cellulose was sufficient, resulting in the formation of larger clusters [22]. The images showed that acid hydrolysis caused deformation of the fibrous, coiled structure of cellulose, leading to the formation of spherical shaped cellulose nanocrystals [23]. The overall particle size of the cellulose nanocrystals ranged from 10 to 100 nm. The cellulose nanocrystals morphology exhibits clumping from the drying process, indicating strong cohesion within the nanomaterials [24]. TEM images of the cellulose nanocrystals obtained are depicted in Fig. 5, revealing consistently spherical shapes with a diameter of 36-79 nm, consistent with previous findings [25-27]. Table-3 presents a comparative morphological characteristics of cellulose nanocrystals obtained from various raw materials and extraction methods.

**Thermal studies:** TG analysis was employed to carry out thermal stability investigations of plant biomass and the resul-

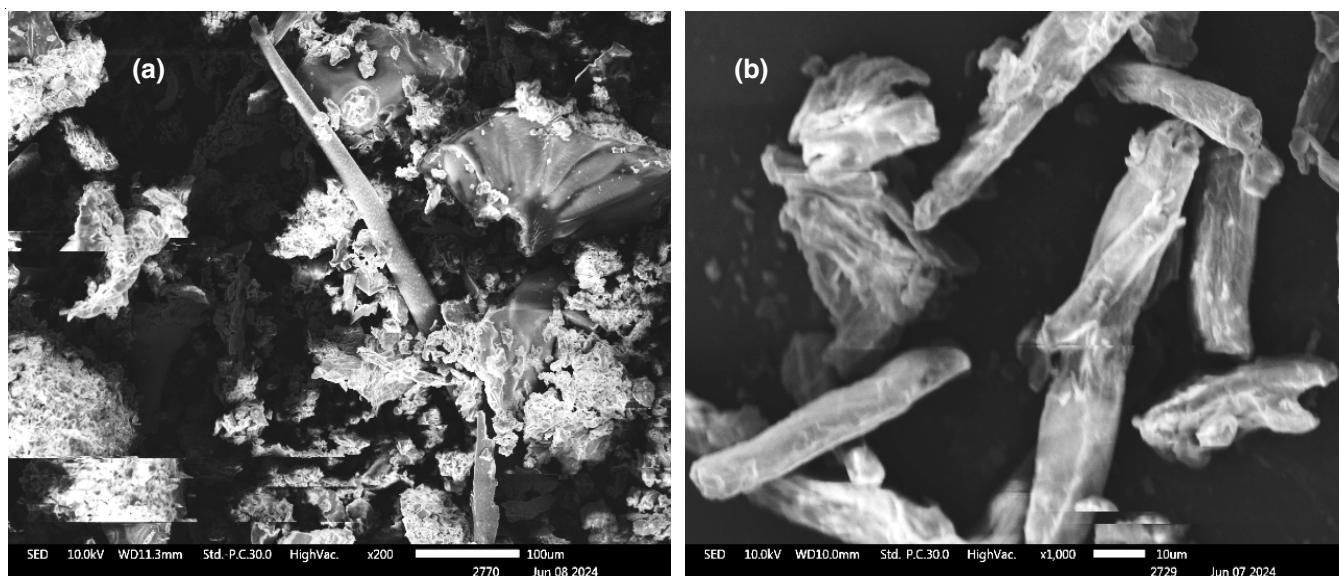


Fig. 3. SEM images of (a) plant biomass (b) cellulose

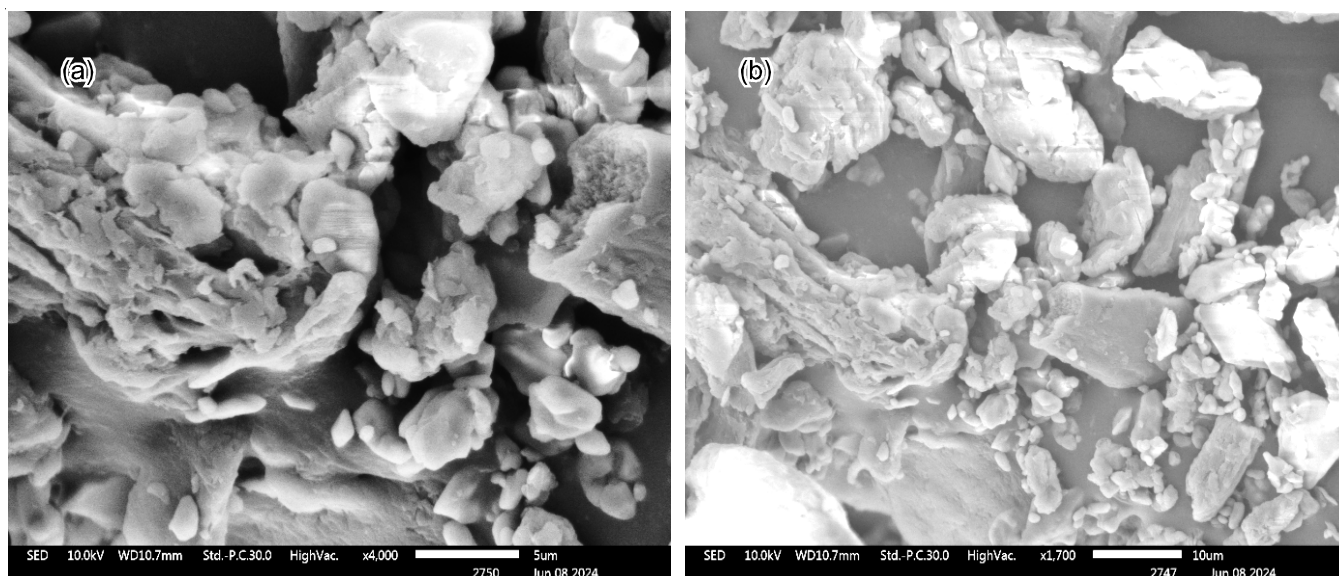


Fig. 4. SEM images of cellulose nanocrystals (a) at 5  $\mu\text{m}$ , (b) 10  $\mu\text{m}$

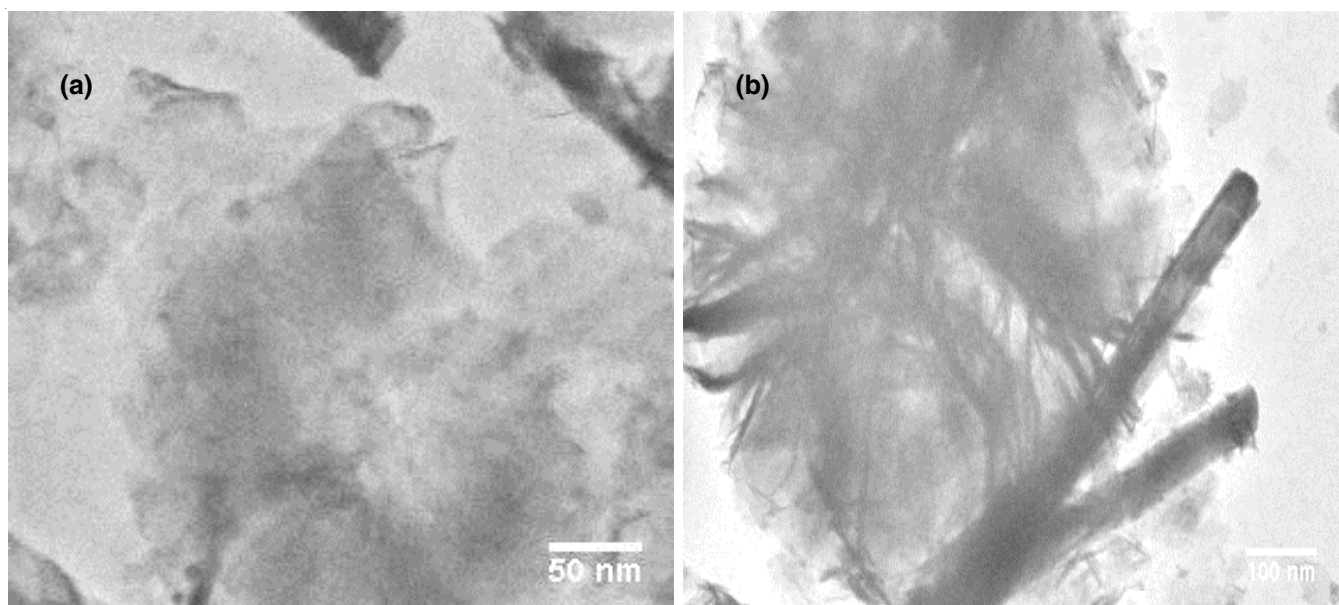


Fig. 5. TEM images of cellulose nanocrystals (a) at 50 nm, (b) 100 nm

TABLE-3  
COMPARISON OF CELLULOSE NANOCRYSTALS (CNCs)  
CHARACTERISTICS OBTAINED FROM VARIOUS RAW  
MATERIALS WITH ACID HYDROLYSIS METHODS

Source	Size (nm)	Morphology	Ref.
Palm waste	42-82	Spherical	[25]
Pine apple peel	11-36	Spherical	[21]
Cellulose nanocrystals from waste cellulose	50	Rod Shape	[15]
Sisal fibre	10-40	Needle Like	[26]
Gai bamboo	2-10	Spherical	[27]
Cotton Pulp	40	Spherical	[23]
Cellulose nanocrystals from <i>Parthenium</i>	20-80	Spherical	This study

ting cellulose nanocrystals. Thermal stability of polymers hinges on both sample intrinsic properties and molecular interactions among macromolecules. The TG thermograms were recorded

from 25 °C to 750 °C under nitrogen at a heating rate of 10 °C/min and the results obtained are depicted in Fig. 6. Plant biomass exhibited weight loss between 300 °C and 400 °C, likely due to glycosyl unit decomposition in cellulose fibers [28,29]. Extracted cellulose and cellulose nanocrystals displayed lower degradation temperatures. Cellulose degradation occurred in two stages *viz.* 150 to 300 °C and 350 to 450 °C, with weight losses of 56% and 27%, respectively, attributed to cellulose depolymerization [21]. In contrast, cellulose nanocrystals showed initial degradation between 130 and 350 °C and a second stage from 350 to 550 °C, with weight losses of 52% and 46%, respectively. Introduction of sulfate groups in cellulose nanocrystals accelerated cellulose depolymerization. These findings highlight that ultrasound-assisted acid hydrolysis enhanced the thermal stability of cellulose nanocrystals compared to raw materials, consistent with literature comparisons [30].

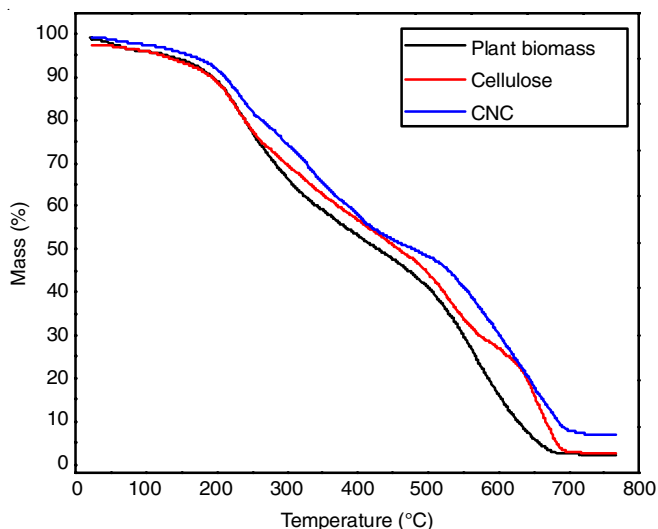


Fig. 6. Thermograms of (a) plant biomass, (b) cellulose and (c) cellulose nanocrystals

#### Particle size distribution of cellulose nanocrystals (CNCs):

Fig. 7 displays the particle size distribution (PSD) of cellulose nanocrystals produced from biomass *via* acid hydrolysis, measured using light scattering. The analysis revealed that most particles fell within the size range of 50 to 700 nm, with smaller particles ranging from 50 to 100 nm. The average size of the cellulose nanocrystals, as determined by PSD analysis, was 217 nm [31].

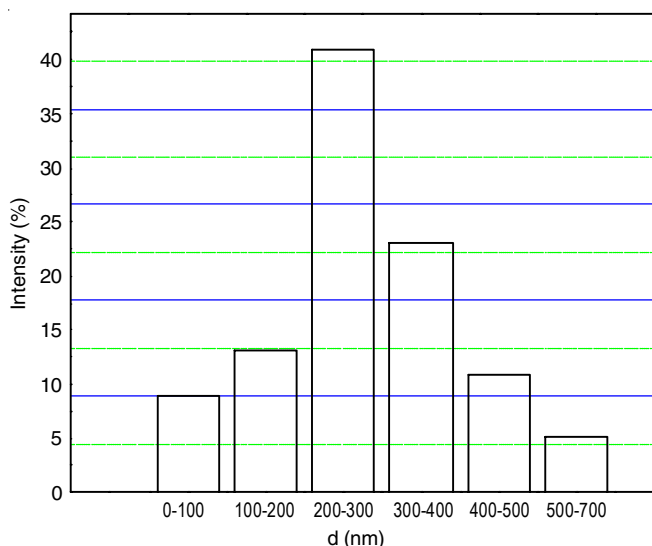


Fig. 7. Particle size distribution of cellulose nanocrystals

**Zeta potential analysis:** Zeta potential analysis revealed that the cellulose nanocrystals exhibited excellent colloidal stability with a highly negative surface charge, approximately  $-28.9 \pm 6.18$  mV. This stability in water dispersion was attributed to the sulfate groups grafted onto the cellulose nanocrystals during sulfuric acid hydrolysis, which enhanced their negative zeta potential [32]. Particles with zeta potentials below  $-30$  mV are known for their stability in solution, preventing aggregation and ensuring a uniform distribution [33,34].

**Adsorption studies:** The cellulose nanocrystals was employed as an effective adsorbent for the removal of malachite

green dye from aqueous solutions. The zero point charge (ZPC) of cellulose nanocrystals was 6-7, indicating a negative surface charge, is particularly advantageous for adsorbing cationic dyes like malachite green. This negative charge is primarily attributed to sulfate groups on the cellulose nanocrystals surface, which electrostatically attract and bind with the positively charged nitrogen atoms of malachite green dye molecules. This interaction is pivotal in the adsorption process, facilitating the removal of malachite green from water. For visual clarity, the proposed adsorption mechanism is depicted in Fig. 8, illustrating the electrostatic binding between cellulose nanocrystals and malachite green dye molecules.

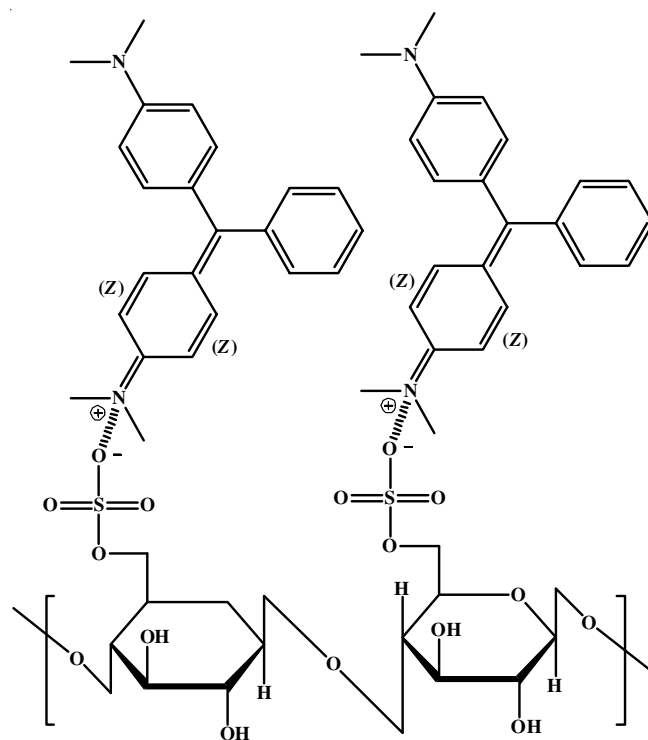


Fig. 8. Proposed mechanism for adsorption of malachite green dye with cellulose nanocrystals as adsorbent

The effect of contact time was systematically investigated over a range of 0 to 120 min across various concentrations, as shown in Fig. 9. The findings indicated that cellulose nanocrystals effectively removed 70-75% of the dye across all tested concentrations. This demonstrates the consistent and reliable adsorption capability of cellulose nanocrystals for malachite green dye removal under varying contact times and concentrations. The rate of adsorption progressively increased with time, average ranging from 20% to 75% during the experimental observations for all concentrations. At lower concentrations, cellulose nanocrystals adsorption sites are quickly occupied because there are fewer dye molecules in the solution competing for these sites. Consequently, saturation occurs sooner (at 60 min) compared to higher concentrations. With increasing concentration, more dye molecules are available to adsorb onto cellulose nanocrystals, requiring longer times to reach equilibrium (around 80 min). The percentage of dye uptake also tends to rise with concentration, reflecting the greater availability of

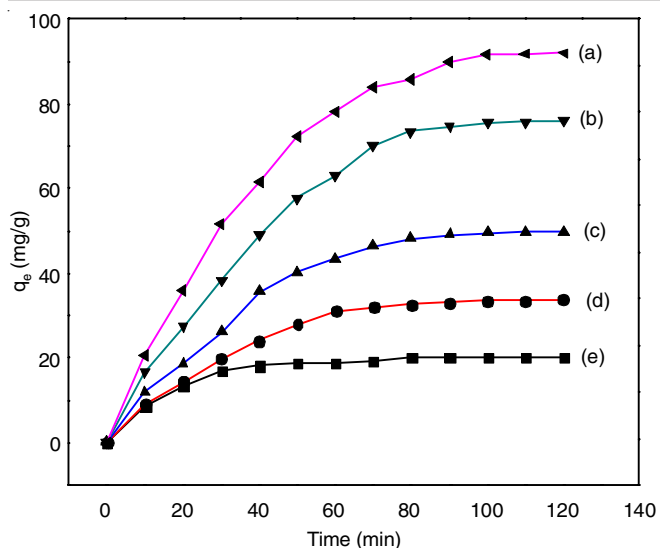


Fig. 9. Effect of contact time on adsorption of malachite green dye on cellulose nanocrystals at (a) 120 ppm (b) 100 ppm (c) 70 ppm (d) 50 ppm (e) 30 ppm

adsorbate molecules. At the lower concentrations, diffusion of adsorbate molecules to the adsorbent surface may occur more rapidly due to the lower molecule density in the solution, contributing to faster adsorption kinetics and quicker attainment of equilibrium.

The experimental data collected in this study were analyzed using nonlinear pseudo-first-order and pseudo-second-order kinetic models. This analytical approach was employed to gain a deeper understanding of the adsorption kinetics involved. The non-linear forms of the pseudo-first-order (eqn. 6) and pseudo-second-order (eqn. 7) kinetic models are given as follows [35]:

$$q_t = q_e(1 - e^{-k_1 t}) \quad (6)$$

$$q_t = \frac{k_2 t q_e^2}{1 + k_2 q_e} \quad (7)$$

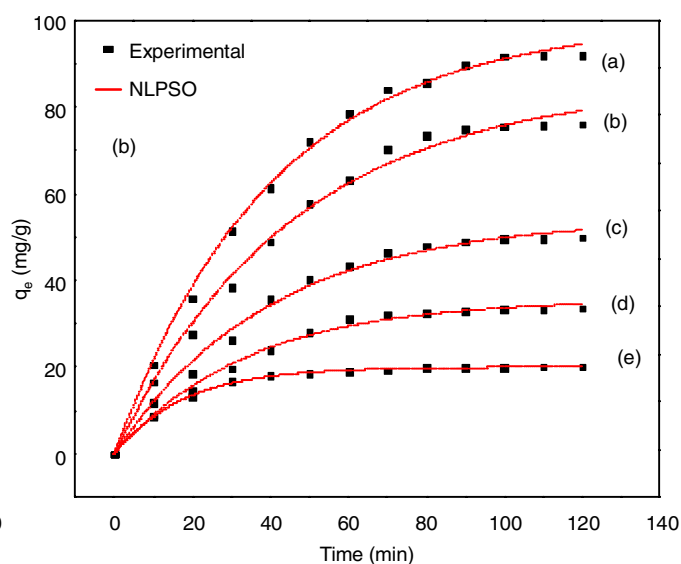
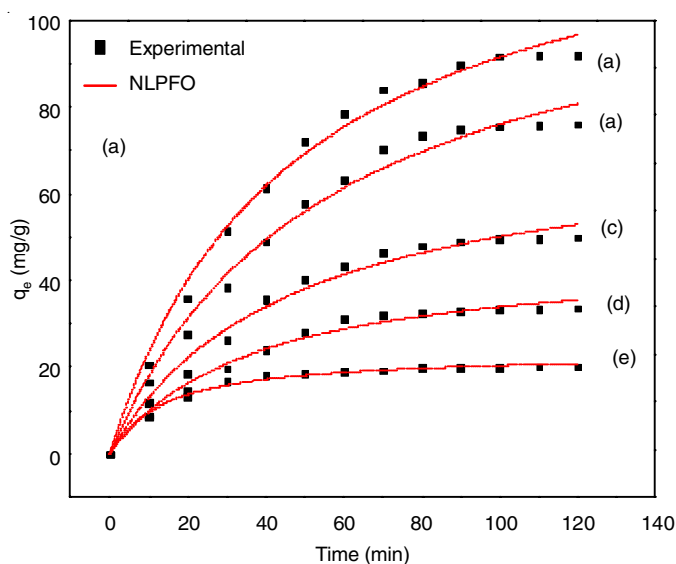


Fig. 10. Non-linear (a) pseudo first order and (b) second order kinetic plots

In these equations,  $q_e$  and  $q_t$  represent the amounts of dye adsorbed on the adsorbent at equilibrium (mg/g) and at time  $t$  (min) (mg/g), respectively. The parameter  $k_1$  ( $\text{min}^{-1}$ ) denotes the pseudo-first-order rate constant, which characterizes the rate of adsorption. On the other hand,  $k_2$  ( $\text{g/mg min}$ ) signifies the pseudo-second-order rate constant, providing a measure of the adsorption rate and capacity of the adsorbent material.

The parameters for the pseudo-first-order and pseudo-second-order kinetic models, respectively, were determined using nonlinear regression in this study. This approach was chosen to accurately model the complex adsorption kinetics observed, ensuring precise estimation of adsorption parameters from experimental data [36].

Fig. 10 illustrates the results of nonlinear regression analysis comparing calculated  $q_e$  values with experimental data. A closer match between experimental and predicted  $q_e$  values across different models indicates better agreement. In this study, experimental values closely aligned with predictions from the nonlinear pseudo-second-order (NLPFO) model, as depicted in Fig. 10b [37,38]. The coefficient of determination ( $R^2$ ) values, which gauge model fit, were significantly high (approaching 1.0) for the PSO equation compared to the nonlinear pseudo-first-order (NLPFO) equation across all tested concentrations, indicating superior performance. The obtained results show a strong correlation with previous studies [39,40]. Kinetic parameters for each model (PFO and PSO) were determined using nonlinear regression and are summarized in Table-4.

## Conclusion

In this study, the synthesized nanocellulose crystals from *Parthenium hysterophorus* biomass through acid hydrolysis, exhibiting its potential as a sustainable nanomaterial. With *P. hysterophorus* biomass boasting a high cellulose content (43.28 %), this invasive weed proves to be a viable and abundant source for nanocellulose production. The synthesized nanocellulose was meticulously characterized using advanced techniques such as SEM, TEM, XRD, FTIR, TGA, particle size distribution analysis and zeta potential measurement. Key findings included

TABLE-4  
PARAMETERS OF DIFFERENT KINETIC MODELS FOR ADSORPTION OF MALACHITE GREEN ON CELLULOSE NANOCRYSTALS

Kinetic model	Parameter	Concentration (ppm)				
		30	50	70	100	120
Pseudo first order (PFO)	$k_1$ ( $\text{min}^{-1}$ )	$5.58 \times 10^{-2}$	$2.8 \times 10^{-2}$	$2.5 \times 10^{-2}$	$2.1 \times 10^{-2}$	$2.4 \times 10^{-2}$
	$q_e$ (mg/g)	23.25	46.60	70.2	103.79	128.59
	$R^2$	0.988	0.984	0.982	0.986	0.991
Pseudo second order (PSO)	$k_2$ (g/mg/min)	$3.0 \times 10^{-3}$	5.7	2.95	1.51	1.57
	$q_e$ (mg/g)	20.08	35.71	54.27	85.21	99.63
	$R^2$	0.994	0.993	0.991	0.992	0.997

the significant enhancement of crystallinity through combined pretreatment and acid hydrolysis processes. SEM and TEM images confirmed morphological changes, with an observed average particle size of approximately 217 nm. Moreover, nanocellulose exhibited improved thermal stability compared to raw biomass following the alkali pretreatment, bleaching and acid hydrolysis. Zeta potential analysis revealed strong colloidal stability with a highly negative surface charge ( $-28.9 \pm 6.18$  mV). In practical applications, the synthesized nanocellulose demonstrated small particle size (50-100 nm), high crystallinity (77%) and stable thermal properties, highlighting its potential in effective dye adsorption. Specifically, nanocellulose removed 75% of malachite green dye from aqueous solutions at room temperature, with adsorption kinetics following pseudo-second-order behaviour supported by high  $R^2$  values. This research significantly advances sustainable materials science by harnessing invasive weed biomass for the production of valuable nanomaterials. The findings underscore the promising applications of *P. hysterophorus* derived nanocellulose in environmental remediation and other industrial sectors, paving the way for further exploration and optimization in future studies.

#### CONFLICT OF INTEREST

The authors declare that there is no conflict of interests regarding the publication of this article.

#### REFERENCES

- Y. Yang, Z. Chen, J. Zhang, G. Wang, R. Zhang and D. Suo, *Int. J. Polym. Sci.*, **39**, 417 (2019); <https://doi.org/10.1155/2019/417427>
- P. Nehra and R.P. Chauhan, *Iran. Polym. J.*, **31**, 771 (2022); <https://doi.org/10.1007/s13726-022-01040-0>
- M. Kaur, P. Sharma and S. Kumari, *J. Nanosci. Nanotechnol.*, **21**, 3394 (2021); <https://doi.org/10.1166/jnn.2021.19006>
- K. Song, X. Zhu, W. Zhu and X. Li, *Bioresour. Bioprocess.*, **6**, 45 (2019); <https://doi.org/10.1186/s40643-019-0279-z>
- L. Chen, N. Reddy and Y. Yang, *Environ. Sci. Technol.*, **47**, 4505 (2013); <https://doi.org/10.1021/es304429s>
- Y.L. Hsieh, *J. Mater. Sci.*, **48**, 7837 (2013); <https://doi.org/10.1007/s10853-013-7512-5>
- S. Nigam, A.K. Das and M.K. Patidar, *J. Environ. Chem. Eng.*, **9**, 105424 (2021); <https://doi.org/10.1016/j.jece.2021.105424>
- R. Aggarwal, A.K. Garg, D. Saini, S.K. Sonkar, A.K. Sonker and G. Westman, *Ind. Eng. Chem. Res.*, **62**, 649 (2023); <https://doi.org/10.1021/acs.iecr.2c03365>
- S. Kumari, D. Mankotia and G.S. Chauhan, *J. Environ. Chem. Eng.*, **4**, 1126 (2016); <https://doi.org/10.1016/j.jece.2016.01.008>
- Y. Xu and M.A. Hanna, *Ind. Crops Prod.*, **32**, 511 (2010); <https://doi.org/10.1016/j.indcrop.2010.06.024>
- F. Beltramino, M.B. Roncero, A.L. Torres, T. Vidal and C. Valls, *Cellulose*, **23**, 1777 (2016); <https://doi.org/10.1007/s10570-016-0897-y>
- A. Kazachenko, F. Akman, M. Medimagh, N. Issaoui, N. Vasilieva, Y.N. Malyar, I.G. Sudakova, A. Karacharov, A. Miroshnikova and O.M.S. Al-Dossary, *ACS Omega*, **6**, 22603 (2021); <https://doi.org/10.1021/acsomega.1c02570>
- U. Holzwarth and N. Gibson, *Nat. Nanotechnol.*, **6**, 534 (2011); <https://doi.org/10.1038/nnano.2011.145>
- M. Mariano, C. Chirat, N. El Kissi and A. Dufresne, *J. Polym. Sci., B, Polym. Phys.*, **54**, 2284 (2016); <https://doi.org/10.1002/polb.24139>
- N. Pandi, S.H. Sonawane and K. Anand Kishore, *Ultrason. Sonochem.*, **70**, 105353 (2021); <https://doi.org/10.1016/j.ultsonch.2020.105353>
- F. Kallel, F. Bettaieb, R. Khiari, A. Garcia, J. Bras and S.E. Chaabouni, *Ind. Crops Prod.*, **87**, 287 (2016); <https://doi.org/10.1016/j.indcrop.2016.04.060>
- S. Bano and Y.S. Negi, *Carbohydr. Polym.*, **157**, 1041 (2017); <https://doi.org/10.1016/j.carbpol.2016.10.069>
- F. Whba, F. Mohamed, M.I. Idris and M.S. Yahya, *Appl. Sci.*, **13**, 6316 (2023); <https://doi.org/10.3390/app13106316>
- O. Romruen, P. Kaewprachu, T. Karbowski and S. Rawdkuen, *Polymers*, **14**, 2534 (2022); <https://doi.org/10.3390/polym14132534>
- Y. Guo, Y. Zhang, D. Zheng, M. Li and J. Yue, *Int. J. Biol. Macromol.*, **163**, 927 (2020); <https://doi.org/10.1016/j.ijbiomac.2020.07.009>
- E.G. Bacha and H.D. Demsash, *PREPRINT Research Square* (2021); <https://doi.org/10.21203/rs.3.rs-296990/v1>
- M. Pan, X. Zhou and M. Chen, *BioResources*, **8**, 933 (2013); <https://doi.org/10.15376/biores.8.1.933-943>
- B. Liu, L. Cheng, Y. Yuan, J. Hu, L. Zhou, L. Zong, Y. Duan and J. Zhang, *Int. J. Biol. Macromol.*, **242**, 124738 (2023); <https://doi.org/10.1016/j.ijbiomac.2023.124738>
- Z. Wang, X. Qiao and K. Sun, *Carbohydr. Polym.*, **197**, 442 (2018); <https://doi.org/10.1016/j.carbpol.2018.06.025>
- S. Mehanny, E.E. Abu-El Magd, M. Ibrahim, M. Farag, R. Gil-San-Millan, J. Navarro, A.E.H. El Habbak and E. El-Kashif, *J. Mater. Res. Technol.*, **10**, 526 (2021); <https://doi.org/10.1016/j.jmrt.2020.12.027>
- J. Agarwal, S. Mohanty and S.K. Nayak, *J. Appl. Polym. Sci.*, **137**, 49291 (2020); <https://doi.org/10.1002/app.49291>
- T.V.V. Do, N.B.A. Tran and N.U. Nguyen-Thai, *Polym. Compos.*, **44**, 2287 (2023); <https://doi.org/10.1002/pc.27243>
- D.L. Vinayaka, V. Guna, D. Madhavi, M. Arpitha and N. Reddy, *Ind. Crops Prod.*, **100**, 126 (2017); <https://doi.org/10.1016/j.indcrop.2017.02.019>
- A.B. Perumal, P.S. Sellamuthu, R.B. Nambiar, E.R. Sadiku, G. Phiri and J. Jayaramudu, *Appl. Clay Sci.*, **158**, 1 (2018); <https://doi.org/10.1016/j.clay.2018.03.008>

30. W.P. Flauzino Neto, H.A. Silvério, N.O. Dantas and D. Pasquini, *Ind. Crops Prod.*, **42**, 480 (2013);  
<https://doi.org/10.1016/j.indcrop.2012.06.041>
31. X. An, Y. Wen, D. Cheng, X. Zhu and Y. Ni, *Cellulose*, **23**, 2409 (2016);  
<https://doi.org/10.1007/s10570-016-0964-4>
32. R.H.F. Faradilla, G. Lee, A. Rawal, T. Hutomo, M.H. Stenzel and J. Arcot, *Cellulose*, **23**, 3023 (2016);  
<https://doi.org/10.1007/s10570-016-1025-8>
33. J.P.S. Morais, M.F. Rosa, M.M. de Souza Filho, L.D. Nascimento, D.M. do Nascimento and A.R. Cassales, *Carbohydr. Polym.*, **91**, 229 (2013);  
<https://doi.org/10.1016/j.carbpol.2012.08.010>
34. D.O. De Castro, J. Bras, A. Gandini and N. Belgacem, *Carbohydr. Polym.*, **137**, 1 (2016);  
<https://doi.org/10.1016/j.carbpol.2015.09.101>
35. D. Gautam, S. Kumari, B. Ram, G.S. Chauhan and K. Chauhan, *J. Environ. Chem. Eng.*, **6**, 3889 (2018);  
<https://doi.org/10.1016/j.jece.2018.05.029>
36. H. Moussout, H. Ahlafi, M. Aazza and H. Maghat, *Int. J. Mod. Sci.*, **4**, 244 (2018);  
<https://doi.org/10.1016/j.kijoms.2018.04.001>
37. R. Nicola, S.-G. Muntean, M.-A. Nistor, A.-M. Putz, L. Almásy and L. Săcărescu, *Chemosphere*, **261**, 127737 (2020);  
<https://doi.org/10.1016/j.chemosphere.2020.127737>
38. R. Batmaz, N. Mohammed, M. Zaman, G. Minhas, R.M. Berry and K.C. Tam, *Cellulose*, **21**, 1655 (2014);  
<https://doi.org/10.1007/s10570-014-0168-8>
39. M.M. Ansari, Y. Heo, K. Do, M. Ghosh and Y.O. Son, *Carbohydr. Polym. Technol. Appl.*, **8**, 100529 (2024);  
<https://doi.org/10.1016/j.carpta.2024.100529>
40. K.A. Kumar, M. Bharath and B.M. Krishna, *Water Pract. Technol.*, **17**, 128 (2022);  
<https://doi.org/10.2166/wpt.2021.106>